ChemElectroChem

Research Article
doi.org/10.1002/celc.202200675

Chemistry Europe
European Chemical Societies Publishing

www.chemelectrochem.org

Special Collection

Gaining the Freedom of Scalable Gas Diffusion Electrodes for the CO_2 Reduction Reaction

Xin Wang[+],[a] Chanikarn Tomon[+],[a, b] Tim Bobrowski,[a] Patrick Wilde,[a] João R. C. Junqueira,[a] Thomas Quast,[a] Wenhui He,[a] Nivedita Sikdar,[a] Jonas Weidner,[a] and Wolfgang Schuhmann*[a]

Dedicated to Prof. Plamen Atanassov on the occasion of his 60th birthday

Gas diffusion electrodes (GDEs) in CO_2 reduction reaction (CO_2RR) alleviate the mass transfer limitation of gaseous reagents, which is beneficial for reducing CO_2 into valuable chemicals. GDEs offer higher current densities compared to electrodes immersed in the electrolyte. Disclosing the roles of different structural parameters in tuning the performance of the GDEs is essential to exert the potential of catalysts and to meet potential large-scale industrial applications of the CO_2RR. A novel layer structure for the airbrush-type spray fabrication of GDEs was designed and optimised, comprising a carbon-based gas-diffusion layer, a PEEK fabric, a Ni mesh, a carbon-integrated catalyst layer, and a PTFE top layer. It was shown that adjusting the carbon material in the gas diffusion and the catalyst layer impacts the selectivity of the CO_2RR due to the modulation of the pore network. This work disclosed a practical and scalable but also an easily transferable pathway for preparing GDEs and offered an idea of how to tune the significant parameters of GDEs for optimising their CO_2RR performance.

Introduction

The electrochemical CO_2 reduction reaction (CO_2RR) powdered by green energy has attracted plenty of research interest due to its potential for sustainable synthesis of chemicals and fuels, such as CO, CH_4, C_2H_4, HCOOH, etc.[1–4] Planar electrodes with comparatively simple configurations were widely employed to evaluate the CO_2RR performances of novel electrocatalysts.[5–8] However, the planar electrodes were immersed into electrolytes leading to mass transport limitations at already small current densities due to the low solubility of CO_2. The reported current densities using planar electrodes are limited to tens of $mA \cdot cm^{-2}$, far from meeting any possible industrial standards (hundreds of $mA \cdot cm^{-2}$).[5,9,10] Moreover, the bubbling of CO_2 into the electrolyte prevents the use of highly alkaline pH values. Therefore, extensive efforts have recently been dedicated to developing gas-fed cells with gas diffusion electrodes (GDEs) for mitigating the restriction of CO_2 mass transport.[11–15]

In contrast to planar electrodes, GDEs are complex systems that require tuning of numerous design parameters to optimise the CO_2RR at the three-phase interface of catalyst, electrolyte, and gaseous CO_2. As shown in Figure 1a, a typical GDE consists of a gas diffusion layer (GDL) and a catalyst layer (CL). The GDL is exposed to the gas supply, and the CL is in contact with the liquid electrolyte.[5,14,16] Typically, the GDL consists of a carbon fibre layer and a microporous layer containing polytetrafluoro-

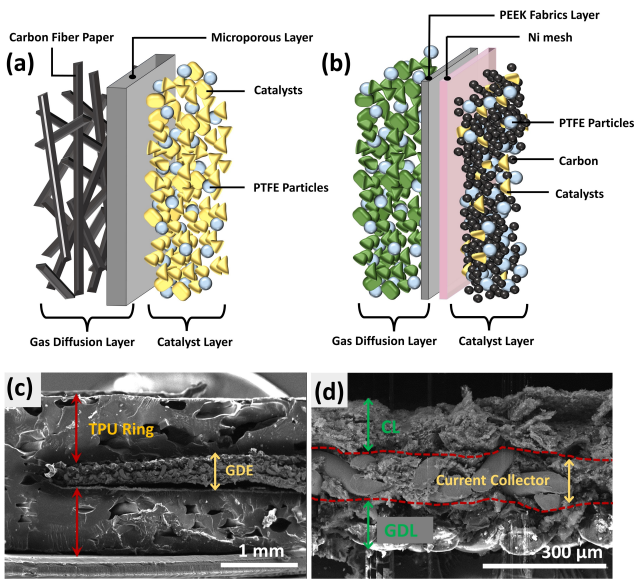

Figure 1. a) Scheme of a typical GDE structure. b) Scheme of the novel GDE design as proposed in this work. SEM cross-section morphology of the GDE at low magnification(c) and high magnification (d).

[a] X. Wang,[+] Dr. C. Tomon,[+] Dr. T. Bobrowski, Dr. P. Wilde, Dr. J. R. C. Junqueira, Dr. T. Quast, Dr. W. He, Dr. N. Sikdar, J. Weidner, Prof. Dr. W. Schuhmann
Analytical Chemistry – Center for Electrochemical Sciences (CES); Faculty of Chemistry and Biochemistry
Ruhr University Bochum
Universitätstr.150, 44780 Bochum, Germany
E-mail: wolfgang.schuhmann@rub.de

[b] Dr. C. Tomon[+]
Department of Chemical and Biomolecular Engineering, School of Energy Science and Engineering
Vidyasirimedhi Institute of Science and Technology
Rayong, 21210, Thailand

[+] These authors contributed equally to this work.

Supporting information for this article is available on the WWW under https://doi.org/10.1002/celc.202200675

Special Collection

An invited contribution to the Plamen Atanassov Festschrift

ethylene (PTFE) particles, which are essential for achieving uniform gas diffusion and for providing a hydrophobic environment to prevent flooding with the electrolyte. The CL is formed by coating a suspension of PTFE and catalyst particles on the microporous layer of the GDL.[17] In this conventional GDE configuration, two inevitable dilemmas are usually encountered during measurements: *i)* the flooding of electrolyte into the CL at high current densities resulting in the loss of the three-phase boundary;[18–20] and *ii)* peeling off the CL layer as the reaction progresses, causing the parasitic H_2 evolution reaction at the increased exposed carbon surface.

One way to solve these challenges is to develop new procedures for the fabrication of GDEs, which add freedom in tuning structural parameters and enable the free arrangement of the GDL, CL, and supporting electrodes to stabilise the GDE structure and hydrophobic nature. In the pursuit of self-made GDE, various gas diffusion layers, such as carbon-based,[18] metal-based (Ag-based, Sn-based),[15,21,22] PTFE-based,[23] and membrane-based structures[24] were employed in many different fields. Among these, carbon-based GDEs are still the most common electrodes owing to their low costs, high conductivity, excellent stability, and flexibility in variety. To realise the free arrangement of different layers, on the one hand, the thickness of the GDEs needs to be adjusted to improve the gas feed and electron transport rate and to modulate the electrolyte film for balancing the CO_2 transport resistance (to the catalysts) and good ionic conductivity within the CL. On the other hand, the porosity and hydrophobicity are two key parameters for GDEs, irrespective of the GDL or the CL, which can be adapted by changing the content of hydrophobic additives (e.g., PTFE) and pore builder (e.g., polymer balls). However, these additives are insulating compounds and thus influence the electrical conductivity of the GDEs, which has to be addressed by adding conductive materials (e.g., carbon black).

In the fabrication of the GDEs, carbon materials were employed widely, imparting good electronic conductivity and chemical resistance and hence improved stability as catalyst support.[18] To realise the fabrication of GDEs, it is necessary to systematically control multiple structural parameters and balance the interaction of various factors.

In this work, we adjust the parameters that can influence the performance of carbon-based GDEs and develop a unified and transferable approach for designing GDEs. A specifically developed airbrush-type spray-coater was used to spray the different layers to fabricate the GDEs.[25,26]

As shown in Figure 1b, we propose a new GDEs configuration that primarily consists of 5 parts, namely a GDL, a PEEK fabric layer (PFL), a Ni mesh, a CL, and a dispersed PTFE layer from bottom to top. As proof of concept, Cu nanoparticles (25 nm) were used as the catalyst in the CL to exclude the unknown influence of other specially designed catalysts. The GDE was covered by two pieces of thermoplastic polyurethane (TPU) rings to prevent gaseous leakage at the side. Moreover, the thickness of the whole GDE was optimised to be around 340 μm, while the CL and GDL are about 120 μm each (Figure 1c–d). We provide a detailed discussion on the effect of the number of layers and elaborate on how to optimise the most influencing parameters and achieve the final structure of the GDEs.

Results and Discussion

An optimised and reliable fabrication of GDEs is achieved by airbrush-type spray coating. The suspensions of the different inks for spray coating were prepared by mixing carbon materials and methylcellulose with water and isopropanol through an Ultra-Turrax. Next, the ink was sprayed on both sides of the Ni mesh and the PEEK fabric mesh using the spray coater (see experimental section). The obtained electrode was placed inside a heated hydraulic press to consolidate the structure and compressed at predefined pressures. Subsequently, the electrode was put in an oven under an ambient atmosphere to remove the pore builder methylcellulose for the formation of pores. Finally, the GDE was obtained by spraying a thin PTFE film on the top. The preparation of a GDE consists of multiple steps, where each has to be optimised to obtain an optimal working GDE.

Optimisation of the number of layers of the GDE

A simple GDE structure was employed at first for spraying GDEs, which consists of a CL, a GDL and a current collector (Ni mesh). The inks for spraying the CL and the GDL were prepared using the same materials. Namely, carbon XPB-633 and methylcellulose were used as the base materials and pore builder, and Cu nanoparticles (25 nm) as catalysts were mixed in the CL.

To evaluate the influence of the thickness, i.e., the number of layers of a GDE on the performance during CO_2RR, carbon GDEs were fabricated with different numbers of sprayed layers (a scheme of fabricating a GDE with four layers is shown in Figure S1). The carbon GDEs were prepared with two layers, three layers, four layers, and five layers (top-left inserts inside Figure 2a–d) corresponding to the average GDE thickness of 130 μm, 173 μm, 214 μm, and 254 μm (Figure S2), respectively.

The CO_2RR activities were determined by applying chronopotentiometrically five different current densities (J) from $-25\ mA\cdot cm^{-2}$ to $-200\ mA\cdot cm^{-2}$ in a three-compartment GDE glass cell under a constant flow of CO_2. As shown in Figure 2, all carbon GDEs showed CO and HCOOH as the main products of CO_2RR. H_2 was also detected for all measured GDE.

The thinnest GDEs fabricated with two layers cannot perform CO_2RR at high current densities. The experiments had to be stopped before applying $-150\ mA\cdot cm^{-2}$ and $-200\ mA\cdot cm^{-2}$ due to electrowetting and flooding caused by potential-driven reduction in the capillary pressure between the electrolyte and GDL substrate.[20] After increasing the GDE thickness to three and four layers, the CO_2RR measurements could be successfully carried out at the predefined current densities up to $-200\ mA\cdot cm^{-2}$, as shown in Figure 2 b-c. The four layers GDE exhibits a higher selectivity for CO_2 reduction products (29.2% CO and 16.0% formic acid at $-50\ mA\cdot cm^{-2}$) and lower H_2 evolution. The five layers GDE (254.4 μm) easily

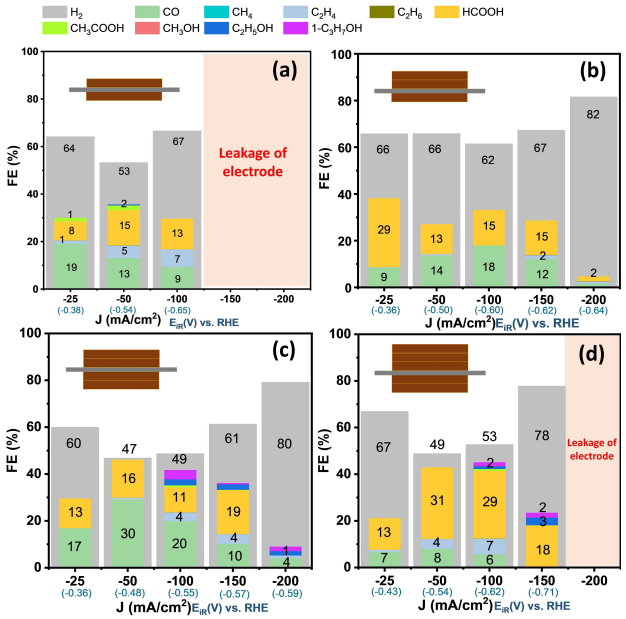

Figure 2. Faradaic efficiency (FE%) for CO_2RR products at different applied current densities (J) of 2 layers (a), 3 layers (b), 4 layers (c), and 5 layers (d) carbon GDE.

cracked during hot-pressing and heating procedures leading to the undesirable leakage of the electrolyte under measuring conditions. Furthermore, when compared to the four layers GDE, the five layers GDE has a denser film at the same pressure during hot-pressing causing lower CO_2 permeability and thus lower CO_2RR activity.[27] Considering that the four layers GDE has the lowest activity towards the competing HER, this electrode structure was employed for further fabrication and characterisation steps.

Electrode porosity

Fast ion bombardment (FIB) was used to expose a cross-section of a four-layers GDE to study the porosity aiming at improving CO_2RR conversion to valuable products. Figure S3 shows the side view of the electrode displaying no visible pores or channels inside the GDE, which supposedly causes inconsistent gas transport and hence limits the possibility of maintaining a stable three-phase boundary within the GDE. Three factors can influence the porosity of the four layers GDEs, namely: *i)* the applied pressure in the hot press at 130 °C, *ii)* the amount of methylcellulose, and *iii)* the employed carbon materials. Four-layers GDEs were fabricated employing different pressures of 100 bar, 300 bar, and 500 bar, respectively, to provide insight into the relationship between the applied hot press pressure and the CO_2RR performance. The GDE fabricated at 100 bar pressure displayed the highest C1 and C2 products (29.2 % CO at $-50\ mA\cdot cm^{-2}$), while the GDEs fabricated with 300 bar and 500 bar exhibited similar CO_2RR activity but higher H_2 production (Figure S4). Figure S4d compares the overpotentials of these three GDEs. The GDE fabricated with 100 bar pressure exhibited the lowest overpotential (-0.39 V vs RHE at $-100\ mA\cdot cm^{-2}$).

We investigated the influence of the amount of pore builder methylcellulose on the GDE porosity and the impact on the GDE performance. Figure S5a shows the H_2 selectivity (FE%) of GDEs sprayed with methylcellulose content of 1 wt%, 1.5 wt%, 2 wt%, and 5 wt% in the four-layers GDE structure, respectively. The GDE with 1 wt% methylcellulose produced the lowest amount of H_2 and the highest total amount of C1 and C2 products (Figure S5b), while the other three GDEs exhibited higher H_2 production and lower C1 and C2 formation. The cross-section of GDEs with 1.5 wt% and 2 wt% methylcellulose (Figure S5c–d) demonstrate little porosity causing poor CO_2RR activity. Obviously, increasing the amount of methylcellulose has little effect on the porosity of the corresponding GDEs. Moreover, increasing amounts of methylcellulose in the spray suspension made the spraying more difficult due to the sticky ink, and more cracks were visible after spraying. Therefore, increasing the methylcellulose amount is not affecting the porosity of the GDEs.

The carbon materials serve as the main skeleton in the GDE structure, ensuring electronic conductivity throughout the electrode and providing mechanical support. The CO_2RR activity and selectivity are significantly affected by the nature of the used carbon material, including particle size, shape, pore structure, and hydrophobicity. The hydrophilic and hydrophobic properties of the carbon materials depend on the nature of the surface groups, which can be altered by various thermal and chemical treatments in the carbon manufacturing processes.[28–30]

Five different carbon types, namely SFG-6, SFG-44, XPB-633, XPB-538, and Super C65, were used to improve the efficiency of the GDEs. The properties of each carbon type are described in Table S1. Figure 3 depicts the product distribution of the GDEs

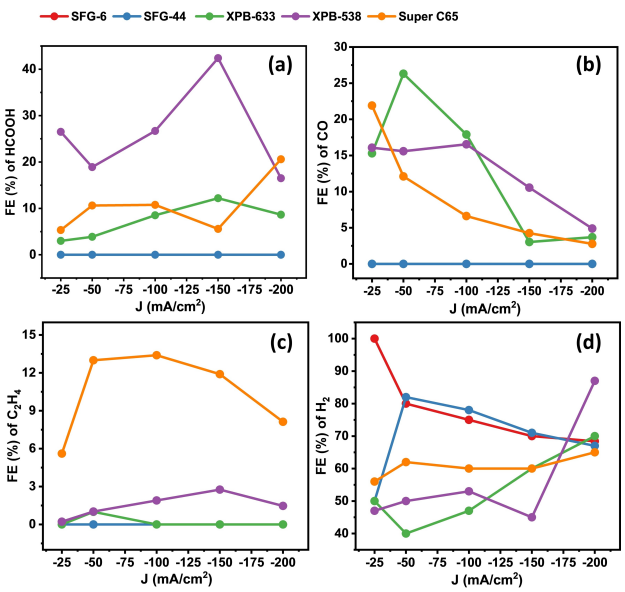

Figure 3. FE of HCOOH (a), CO (b), C_2H_4 (c), and H_2 (d) of the different carbon types.

fabricated using different types of carbon materials. The XPB-538 provides the highest HCOOH selectivity (43% selectivity at $-150\ mA\cdot cm^{-2}$), while it shows low selectivities for C_2H_4 and CO. The XPB-633 carbon GDE shows the highest selectivity towards CO (26% at $-50\ mA\cdot cm^{-2}$) and some formation of HCOOH (12% FE at $-150\ mA\cdot cm^{-2}$), while producing very small amounts of C_2H_4. Interestingly, Super C65 presents a moderate %FE for CO production (26% at $-50\ mA\cdot cm^{-2}$), HCOOH (21% at $-200\ mA\cdot cm^{-2}$), but also the highest selectivity for C_2H_4 (up to 14% at $-100\ mA\cdot cm^{-2}$). Parasitic HER (Figure 3d) is monitored due to its impact on the efficiencies of the CO_2RR. XPB-538 and XPB-633 display a similar amount of HER in the range of 40% to 60% at -25 to $-150\ mA\cdot cm^{-2}$. The graphite type carbon SFG-44 and SFG-6 do not show the formation of any CO_2RR products with almost 100% FE for H_2 formation. According to these results, XPB-538, XPB-633, and Super C65 were found to be suitable for GDE fabrication with selectivities for HCOOH, CO, and C_2H_4, respectively. Since we focus on high selectivity towards C_2 products in this work, we chose Super C65 as carbon component.

To further understand which characteristic of the GDEs fabricated using different carbon materials influences the selectivity towards CO_2RR, the water contact angle and porosity (%) of the different carbon materials were investigated as shown in Figure 4 and Figure S6, respectively.

The hydrophobicity is an essential factor for preventing electrode flooding, enabling CO_2 gas transport, and leading to the formation of the three-phase boundary where the CO_2RR occurs.[5,20] The GDE based on carbon material XPB-633, XPB-538, Super C65, SFG-6, and SFG-44 reveal contact angles of 140.7°, 141.1°, 145.6°, 135.3°, and 135.1°, respectively (Figure S6) with the higher water-contact angle value indicating higher hydrophobicity. The cross-sectional SEM images of the FIB processed GDEs (Figure 4) provide valuable insight into the pore structure. The porosity was calculated based on the pore area ratio divided by the area of total electrode area of interest. SFG-6 and SFG-44 provide the largest pore size and the highest porosity (about 23%). The other carbon types yielded smaller porosity with 11.2% for XPB-538, 10.2% for XPB-633, and 18.5% for Super C65. This suggests that SFG-6 and SFG-44 are best suitable as the bottom part of the GDE, allowing high CO_2 transport through the structure. The smaller pore size of XPB-538, XPB-633, and Super C65 can be advantageously used in the top part of the GDE to prevent electrolyte flooding. Super C65 exhibits the highest porosity of 18% facilitating CO_2 transportation through the GDE. Based on these findings, we used Super C65 to prepare the CL (smaller pore structure) and SFG-6 or SFG-44 to prepare the GDL (bigger pore structure) of GDEs in the following experiments.

Hybrid structure of GDEs

After finding the suitable carbon materials for fabricating the GDL and the CL layers, a hybrid GDE structure was conceived to enhance the GDE performance, as shown in Figure 5b. The bottom or GDL layer consists of SFG-44, methylcellulose, and PTFE as carbon source, pore builder, and hydrophobic material, respectively. The top layer or CL layer of the GDE is prepared in a similar way as the GDL layer but using Super C65 as the carbon material and adding 10 wt% Cu nanoparticles as the catalyst. The FE for H_2 production of the hybrid GDE is in the range of 48–61%, which is the lowest selectivity for H_2. Furthermore, the FE for CO_2RR products increased. The formation of C_2H_4 increases from 6% to 17.4% along with higher applied current densities, while the FE of CO decreases with the increasing potential. The increased potential is leading to electrolyte flooding of the GDE, promoting the parasitic HER.[31] The HCOOH formation raises from 15.5% at

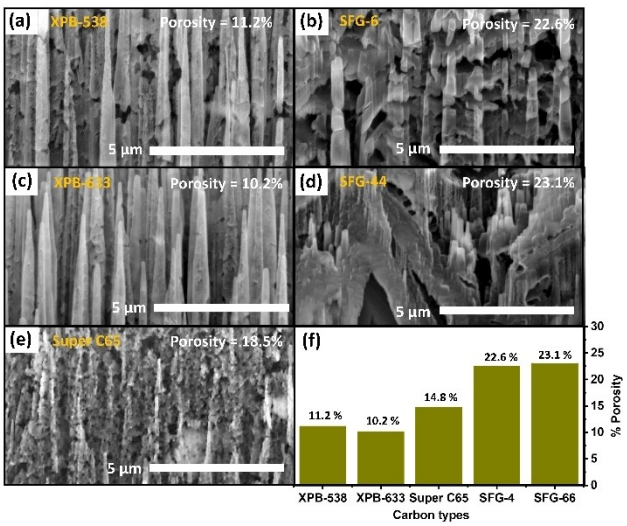

Figure 4. The porosity (%) of the as-prepared GDEs using carbon source of XPB-538 (a), SFG-6 (b), XPB-633 (c), SFG-44 (d), Super C65 (e), and plotting between porosity (%) and carbon types (f).

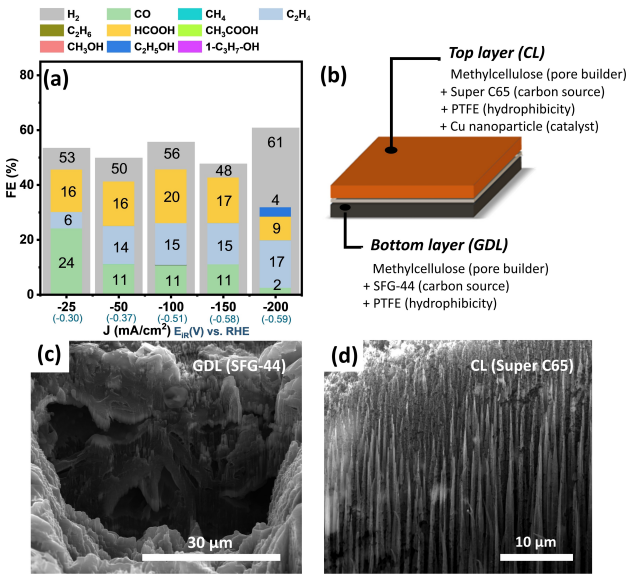

Figure 5. a) FE of the hybrid GDE. b) Scheme of the hybrid GDE configuration. c) SEM image of the GDL using SFG-44. d) Cross-sectional SEM image of the CL using Super C65.

$-25\ mA\cdot cm^{-2}$ to 19.6% at $-100\ mA\cdot cm^{-2}$, and then decreases to 8.6% at $-200\ mA\cdot cm^{-2}$. Noticeably, the low CO_2RR performance and high HER occurred only at a high current density ($-200\ mA\cdot cm^{-2}$) which is caused by electrowetting.[18] The hybrid structure of the GDE enhances the CO_2RR performance. It reduces the parasitic HER as a result of the combination of the larger pore structure of SFG-44 (Figure 5c) in the GDL and the smaller pore structure of Super C65 (Figure 5d) in the CL.

Increasing porosity by pore builder variation

A latex material (polystyrene beads with different particle sizes) was used to improve the porosity and pore size of the hybrid structure GDE. Figure 6a shows the latex particles with 200 nm size mixed in the as-prepared GDE. After heating the GDE to 330 °C to remove the latex, pores were formed in the GDE structure, as shown in Figure 6b. The top SEM image of the GDE based on methylcellulose as a pore builder (Figure 6c) shows a considerably lower porosity than the GDE prepared with latex as a pore builder (Figure 6d). As expected, the higher porosity and larger pore size of the GDE employing latex as the pore builder improves the CO2RR performance significantly (Figure 6e) and suppresses the HER further to a FE of 29% at $-25\ mA\cdot cm^{-2}$ (Figure 6e). This HER selectivity is 54.6% lower than for the hybrid structure GDE using methylcellulose as the pore builder (Figure 5). The increased CO_2RR and decreased HER are observed at all current densities. HCOOH and CO formation show a similar trend with the maximum FE being found at $-25\ mA\cdot cm^{-2}$ (CO 26.2%, HCOOH 20.6%). Both FEs are decreasing when the potential increases. The C_2H_4 formation increased from 14.1% (at $-25\ mA\cdot cm^{-2}$) to 21.5% at $-100\ mA\cdot cm^{-2}$, lowering at higher current densities. These results clearly illustrate that the pore size and the porosity of the GDEs play a major role in the CO_2RR performance. The large pore size and high porosity not only facilitate the CO_2 mass transport but also provide larger areas of the three-phase boundary inside the GDE.

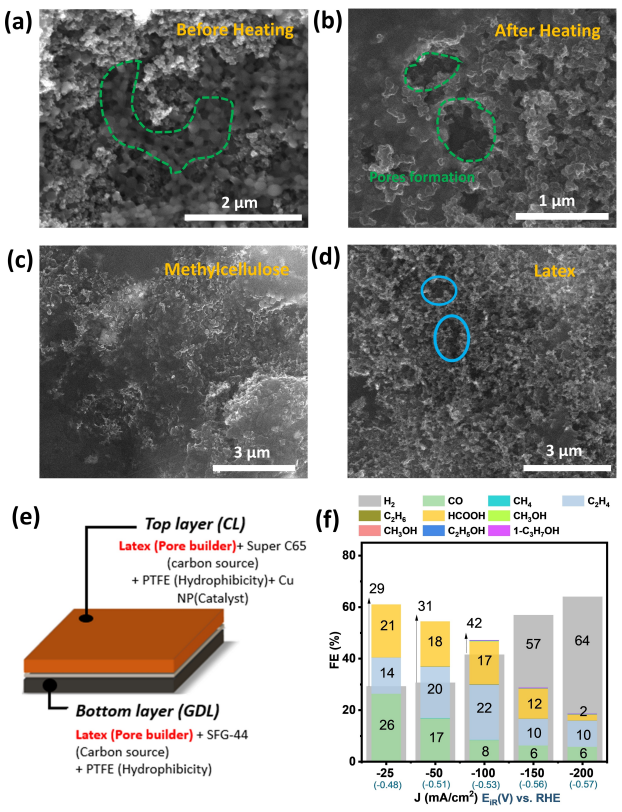

Figure 6. a) SEM image of the hybrid GDE using latex as pore builder before heating at 330 °C. b) SEM image of the as-prepared GDE after heating to 330 °C. c) SEM image of a GDE using methylcellulose as pore builder with low magnification. d) SEM image of a GDE using latex as pore builder with low magnification. e) CO_2RR product in %FE of the hybrid GDE using latex as pore builder.

Application of a PEEK fabric to suppress HER

A PEEK fabric layer (PFL) was introduced between the Ni mesh and the GDL to avoid electrolyte flooding into the GDL and further increase the selectivity towards valuable CO_2RR products and suppress the HER. Additionally, a PTFE layer was added to the CL since exposed carbon active sites enabled the parasitic HER. Figure 7a shows the final structure of the GDE, which consists of GDL, PFL, Ni mesh, CL, and PTFE layer from bottom to top.

For the GDL, SFG-44 carbon was mixed with methylcellulose and latex beads with a diameter of 1 µm to create larger channels, ultimately resulting in an improved pore distribution, which is beneficial for the gaseous CO_2 transport. Carbon Super

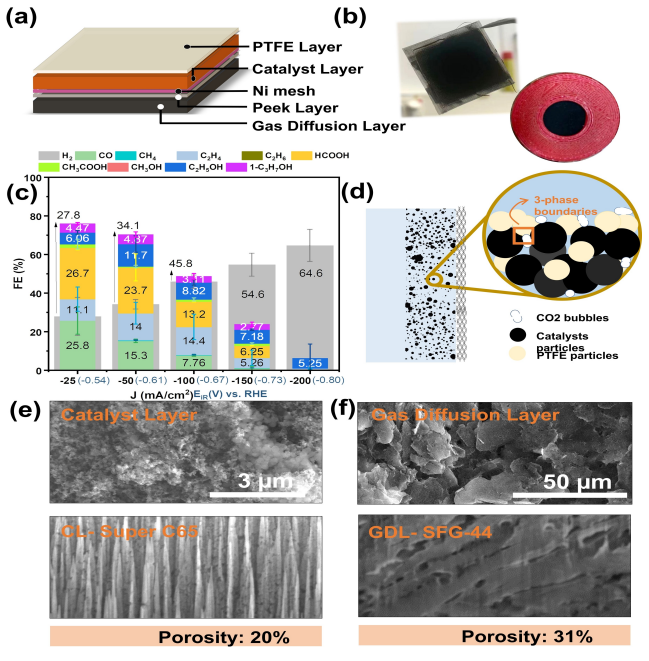

Figure 7. a) The final structure of the GDE after integrating a PFL and a PTFE layer on the top. b) Pictures of the GDE before and after applying TPU rings to cover the side. c) The CO_2RR FE with error bar and overpotential for the final structure of the GDE. Error bars represent the standard deviation between 3 measurements. d) The inner microenvironment around catalyst particles in the CL. SEM images and porosity distribution of e) the CL and f) the GDL.

C65 was used in the CL in combination with latex beads with a diameter of 200 nm, causing smaller pores around the catalyst particles to let electrolyte soak in without flooding the CL.

The CO_2RR activity was measured to determine the performance (Figure 7c). The potential traces (before iR correction) over time and the corresponding galvanostatic EIS data were shown in Figure S7. The formation of C1 and C2 products increased while HER was further suppressed. Compared to the GDE without PFL and PTFE layer, these GDEs produce more CO_2RR products with about 65% FE at $-50\ mA\cdot cm^{-2}$, and more C2 products like ethanol are formed at higher current densities of $-100\ mA\cdot cm^{-2}$. HER was suppressed further, especially at higher current densities due to the integration of the PEEK fabric and the PTFE layer on the top. The overpotential at $-100\ mA\cdot cm^{-2}$ using Cu nanoparticles as catalyst is −0.67 V vs RHE, which is comparatively low and is attributed to the more hydrophobic microenvironment (Figure 7d). As shown in Figure S8, we observed that Cu and C are distributed evenly in the cross-section of the CL, which is a prerequisite for a well-formed three-phase boundary created by the solid catalyst, liquid electrolyte, and gaseous CO_2.

The cross-section SEM images obtained after FIB milling reveal the porosity distribution inside the GDE. Figure 7e shows the porosity distribution of the surface and the cross-section of the CL. The pores with a size of several hundred nanometers are distributed uniformly in the whole CL and display a porosity ratio of about 20% in the cross-section. There are significant more distinct bigger channels inside the GDL with a porosity ratio of 31%, which is beneficial for the gas transport going through the GDL. The water contact angle is an essential measure of the hydrophobicity of the GDE surface.[19] As shown in Figure S8, the contact angle before CO_2RR of the CL was 146.3°, demonstrating a high hydrophobicity and hence ability to repel the liquid electrolyte during the measurement. Figure S9 shows the elemental mapping of the cross-section of the GDL with the carbon and PTFE particles distributed evenly and display the morphology of graphite sheets. The water contact angle of the GDL is 134.8°, which also shows high hydrophobicity, which is essential to avoid electrolyte flooding at high current densities.

Conclusion

We systematically elaborated the process of spray-fabricating carbon-based GDEs by adjusting a series of parameters, which are critical for their performance. The suggested GDE structure comprised five components and provided robust mechanical support for catalysts while simultaneously creating a suitable microenvironment for the three-phase boundary. The GDEs were evaluated using Cu nanoparticles as model catalyst embedded in the CL with a loading of $0.2\ mg\,cm^{-2}$. High selectivity for C1 and C2 products with a FE of about 70% at −0.61 V vs RHE was obtained. The focus of this work was to provide rational suggestions for selecting and optimising the crucial parameters of the most influencing factors on the performance of the GDE. The fabrication process of GDEs reported here provided insights into factors influencing the porosity distribution and structure of the GDEs, which finally lead to improved CO_2RR performance and a lower overpotential. Understanding the function and influencing factors of different components of the GDL, the CL, and the current collector is beneficial for designing the GDE for the CO_2RR or other gas-feeding reactions.

Experimental Section

Ink preparation

Two different inks were prepared separately using different carbon materials used in the CL and the GDL. For the GDL, the spray suspension was prepared by mixing methylcellulose (1.744 g, 1 wt.%), latex beads with a diameter of 1 μm (1.744 g, 1 wt.%), isopropanol (2.006 g), water (1.338 g), carbon SFG-44 (0.097 g), and PTFE dispersion (3 M Dyneon PTFE Dispersion TF 5060GZ, 0.111 g). The ink is stirred under sonication using a magnetic stirring bar for 10 min using an Ultra-Turrax at the same time. The ink for the CL is prepared using methylcellulose (1.744 g, 1 wt%), latex beads with a diameter of 0.2 μm (1.744 g, 1 wt%), isopropanol (2.006 g), water (1.338 g), carbon Super C65 (0.097 g), and PTFE dispersion. The ink for the PTFE layer on the top is prepared by dispersing PTFE (0.058 g) in 30 mL water.

GDE fabrication process

The GDE was prepared by a spray-coating method. As shown in Scheme 1, the cut Ni mesh (3 cm × 3 cm) was stacked with a piece of PEEK fabric layer (3 cm × 3 cm) as the spray support. The GDL and CL are spayed on both sides of the spray support separately. Spray coating was performed using an x/y-axis length of 22 mm, an x/y-axis distance between each spray point of 2 mm, a spraying speed of 8 mm/s, and a volume per position of 8 μL, an aspiration speed of 25 μL/s, a dispensing speed of 6 μL/s. We define one spray layer as spraying from the first x/y position to the last x/y position of the grid. The GDL was first sprayed on the PFL side (two layers). The half-prepared sample was flipped over to spray the CL (2 layers) on the other side onto the Ni mesh.

After spraying, the GDE was placed between two heated plates in the hot press with a pressure of 100 bar and a temperature of 130 °C. Subsequently, the prepared electrode was heated in the oven under an ambient atmosphere at a temperature of 330 °C overnight. As the last step of the GDE preparation, a thin PTFE layer was sprayed on top of the CL using the same spray parameters. Finally, the GDE is cut to a circular shape with a diameter of 18 mm before embedding it between two pieces of TPU rings. The final GDE shown in Scheme 1.

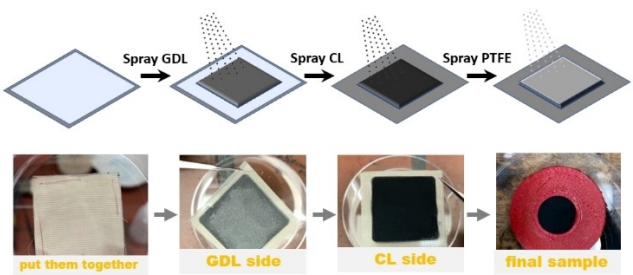

Scheme 1. GDE fabrication process.

Electrochemical measurements

The CO_2RR measurements were performed in a custom-made H-type glass cell (Figure S10). The cell was separated into two compartments by an anion exchange membrane (AEM, FAB-PK-75, Fumatech). The cathode compartment was equipped with the working electrode (GDE) and the reference electrode (Ag/AgCl, 3 M KCl), while the anode compartment contained a Ni foam counter electrode. The geometric surface area of the working electrode is 1.13 cm^2. CO_2 (20 mL min^{-1}) as the reactant was supplied to the GDE from the GDL side, and N_2 (16 mL min^{-1}) was bubbled through the electrolyte of the cathode compartment. The cathode and anode compartments were both filled with 1 M KOH (15 mL in the cathode compartment and 14 mL in the anode compartment). Chronopotentiometry was conducted, followed by galvanostatic EIS measurement at different applied currents using an Autolab potentiostat/galvanostat. The applied current densities were −25, −50, −100, −150, and −200, −250 mA·cm^{-2}, respectively, with the corresponding currents of −2.82, −5.65, −11.30, −16.95, and −22.60 mA, respectively. Considering that the gaseous products can be collected on the gas side and the electrolyte side of the GDE, both outlets were connected via a 6-way selection valve to the gas chromatograph. During the measurement at one current density, the valve was switched between the top chamber where the gaseous products were released into the N_2-purged electrolyte and the bottom chamber where the CO_2 feed to the GDE is flowing. The overpotential (vs. RHE) was calculated using $E_{RHE} = E_{Ag/AgCl\ (3\,M\,KCl)} + 0.210 + 0.059$ pH. All potentials were further iR corrected with the uncompensated solution resistance derived from the galvanostatic EIS at each current density. We evaluated the error range of the overall measurement sequence to be about ±10% for the FE including changes in the CO_2 flux, the loss of CO_2 due to CO_3^{2-} formation, the temperature dependence of the injection volume, variations of backpressure etc. from several 100 GDE measurements. This error range is assumed to be also true for the present study as also demonstrated in Figure 7.

Acknowledgements

This project has received funding from the European Research Council (ERC) under the European Union's Horizon 2020 research and innovation program (grant agreement CasCat [833408]) and from the Deutsche Forschungsgemeinschaft (DFG, German Research Foundation) in the framework of the research unit FOR 2397e2 (276655237) and under Germany's Excellence Strategy-EXC 2033-390677874-RESOLV. X. W. acknowledges the CSC for a PhD fellowship. Open Access funding enabled and organized by Projekt DEAL.

Conflict of Interest

The authors declare no conflict of interest.

Data Availability Statement

The data that support the findings of this study are available from the corresponding author upon reasonable request.

Keywords: CO_2 reduction reaction · electrocatalysis · gas diffusion electrode · GDE design · three-phase boundary

[1] D. T. Whipple, P. J. A. Kenis, *J. Phys. Chem. Lett.* **2010**, *1*, 3451.
[2] H.-R. Jhong, S. Ma, P. J. A. Kenis, *Curr. Opin. Chem. Eng.* **2013**, *2*, 191.
[3] D. W. Keith, G. Holmes, D. St Angelo, K. Heidel, *Joule* **2018**, *2*, 1573.
[4] Á. Vass, B. Endrődi, C. Janáky, *Curr. Opin. Chem. Eng.* **2021**, *25*, 100621.
[5] Z. Xing, L. Hu, D. S. Ripatti, X. Hu, X. Feng, *Nat. Commun.* **2021**, *12*, 136.
[6] Q. Lu, J. Rosen, Y. Zhou, G. S. Hutchings, Y. C. Kimmel, J. G. Chen, F. Jiao, *Nat. Commun.* **2014**, *5*, 3242.
[7] C. W. Li, M. W. Kanan, *J. Am. Chem. Soc.* **2012**, *134*, 7231.
[8] Y. Wu, Z. Jiang, X. Lu, Y. Liang, H. Wang, *Nature* **2019**, *575*, 639.
[9] C. W. Li, J. Ciston, M. W. Kanan, *Nature* **2014**, *508*, 504.
[10] S. Verma, B. Kim, H.-R. M. Jhong, S. Ma, P. J. A. Kenis, *ChemSusChem* **2016**, *9*, 1972.
[11] F. P. García de Arquer, C.-T. Dinh, A. Ozden, J. Wicks, C. McCallum, A. R. Kirmani, D.-H. Nam, C. Gabardo, A. Seifitokaldani, X. Wang, Y. C. Li, F. Li, J. Edwards, L. J. Richter, S. J. Thorpe, D. Sinton, E. H. Sargent, *Science* **2020**, *367*, 661.
[12] T. Burdyny, W. A. Smith, *Energy Environ. Sci.* **2019**, *12*, 1442.
[13] C.-T. Dinh, T. Burdyny, M. G. Kibria, A. Seifitokaldani, C. M. Gabardo, F. P. García de Arquer, A. Kiani, J. P. Edwards, P. de Luna, O. S. Bushuyev, C. Zou, R. Quintero-Bermudez, Y. Pang, D. Sinton, E. H. Sargent, *Science* **2018**, *360*, 783.
[14] S. Ma, M. Sadakiyo, R. Luo, M. Heima, M. Yamauchi, P. J. Kenis, *J. Power Sources* **2016**, *301*, 219.
[15] B. Kim, F. Hillman, M. Ariyoshi, S. Fujikawa, P. J. Kenis, *J. Power Sources* **2016**, *312*, 192.
[16] E. Irtem, T. Andreu, A. Parra, M. D. Hernández-Alonso, S. García-Rodríguez, J. M. Riesco-García, G. Penelas-Pérez, J. R. Morante, *J. Mater. Chem. A* **2016**, *4*, 13582.
[17] Q. Wang, H. Dong, H. Yu, H. Yu, *J. Power Sources* **2015**, *279*, 1.
[18] K. Yang, R. Kas, W. A. Smith, T. Burdyny, *ACS Energy Lett.* **2021**, *6*, 33.
[19] R. Shi, J. Guo, X. Zhang, G. I. N. Waterhouse, Z. Han, Y. Zhao, L. Shang, C. Zhou, L. Jiang, T. Zhang, *Nat. Commun.* **2020**, *11*, 3028.
[20] M. Li, M. N. Idros, Y. Wu, T. Burdyny, S. Garg, X. S. Zhao, G. Wang, T. E. Rufford, *J. Mater. Chem. A* **2021**, *9*, 19369.
[21] W. Luo, J. Zhang, M. Li, A. Züttel, *ACS Catal.* **2019**, *9*, 3783.
[22] S. Sen, S. M. Brown, M. Leonard, F. R. Brushett, *J. Appl. Electrochem.* **2019**, *49*, 917.
[23] R. Lin, J. Guo, X. Li, P. Patel, A. Seifitokaldani, *Catalysts* **2020**, *10*, 473.
[24] M. Wang, S. Medina, J. R. Pfeilsticker, S. Pylypenko, M. Ulsh, S. A. Mauger, *ACS Appl. Energ. Mater.* **2019**, *2*, 7757.
[25] P. Holzapfel, M. Bühler, C. van Pham, F. Hegge, T. Böhm, D. McLaughlin, M. Breitwieser, S. Thiele, *Electrochem. Commun.* **2020**, *110*, 106640.
[26] K. Ehelebe, N. Schmitt, G. Sievers, A. W. Jensen, A. Hrnjić, P. Collantes Jiménez, P. Kaiser, M. Geuß, Y.-P. Ku, P. Jovanovič, K. J. J. Mayrhofer, B. Etzold, N. Hodnik, M. Escudero-Escribano, M. Arenz, S. Cherevko, *ACS Energy Lett.* **2022**, *7*, 816.
[27] S. Hernandez-Aldave, E. Andreoli, *Catalysts* **2020**, *10*, 713.
[28] M. Weissmann, S. Baranton, J.-M. Clacens, C. Coutanceau, *Carbon* **2010**, *48*, 2755.
[29] O. L. Li, L. Qin, N. Takeuchi, K. Kim, T. Ishizaki, *Catal. Today* **2019**, *337*, 155.
[30] A. Lee, S. Beak, S. Lee, G. Kim, D. Lee, S. Kim, Y. Sung, H. Jeong, *Diamond Relat. Mater.* **2020**, *110*, 108152.
[31] X.-F. Qiu, H.-L. Zhu, J.-R. Huang, P.-Q. Liao, X.-M. Chen, *J. Am. Chem. Soc.* **2021**, *143*, 7242.

Manuscript received: June 19, 2022
Revised manuscript received: September 28, 2022
Accepted manuscript online: October 1, 2022